

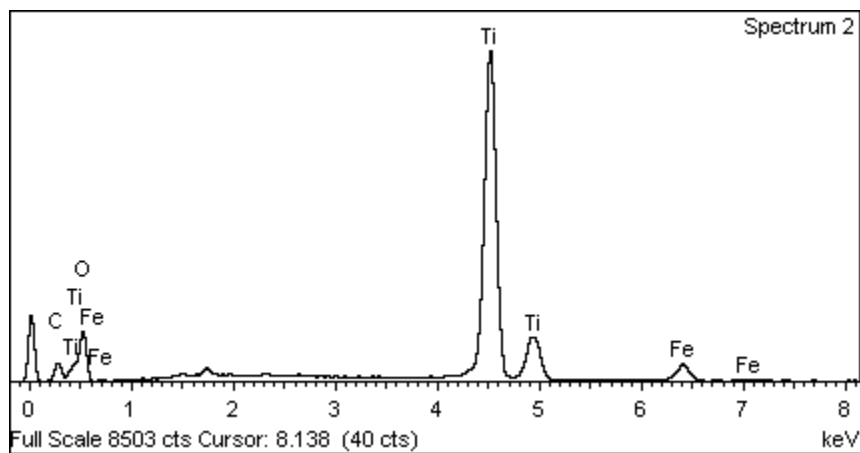
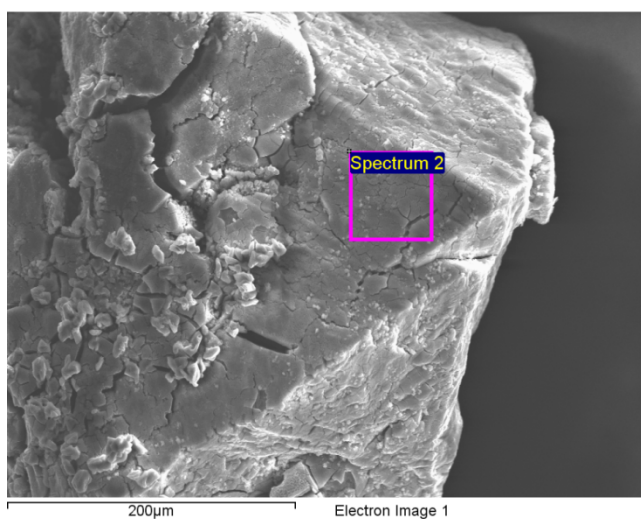
## Supporting Information

# The Optical Properties of Metal-doped Polyoxotitanium Cages and the Relationship to Metal-doped Titania

Yaokang Lv, Jun Cheng, Peter D. Matthews, Juan Pedro Holgado, Janina Willkomm, Michal Leskes, Alexander Steiner, Dieter Fenske, Timothy C. King, Paul T. Wood, Lihua Gan, Richard M. Lambert and Dominic S. Wright

### Section ESI-1 SEM-EDS Results on Crystalline Samples of 2 and 3

#### Compound 2



Spectrum processing :

Peaks possibly omitted : 1.500, 1.741, 2.310 keV

Processing option : All elements analyzed (Normalised)

Number of iterations = 5

Standard :

C CaCO<sub>3</sub> 1-Jun-1999 12:00 AM

O SiO<sub>2</sub> 1-Jun-1999 12:00 AM

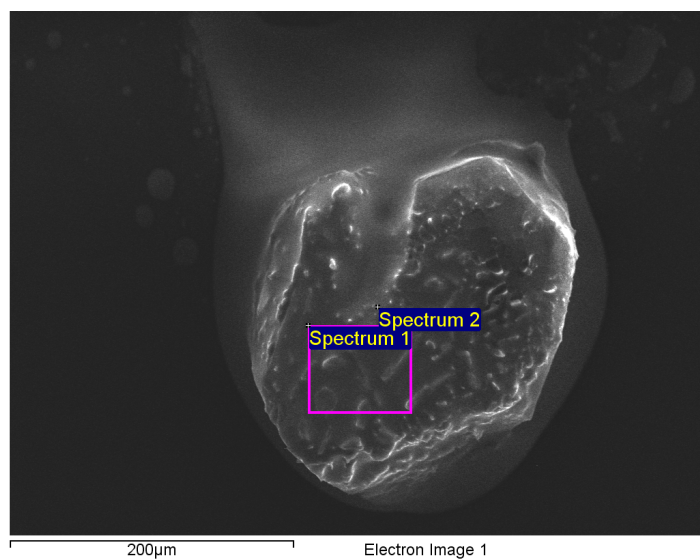
Ti Ti 1-Jun-1999 12:00 AM

Fe Fe 1-Jun-1999 12:00 AM

Element	Weight%	Atomic%
C K	9.60	17.33
O K	46.46	63.00
Ti K	40.36	18.28
Fe K	3.58	1.39
Totals	100.00	

**The Fe : Ti Atomic ratio is 1.39 : 18.28 = 1 : 13.15.**

### Compound 3



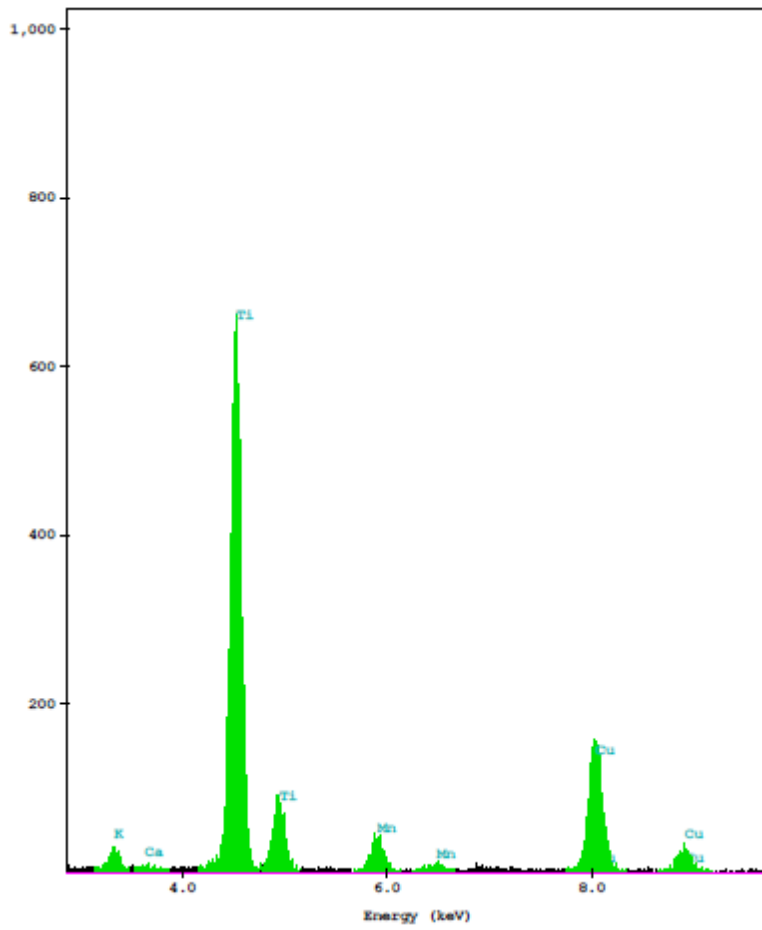
Element	Weight%	Atomic%
C K	9.60	42.25
O K	46.46	50.02
Ti K	40.36	6.29
GaK	3.58	0.44
Totals	100.00	

**The Ga : Ti Atomic ratio is  $0.44 : 6.29 = 1 : 14.30$ .**

#### Section ESI-2 TEM-EDS on 5.

The TEM-EDS results on **5** are presented below. No quantitative determination of the ratio of K : Mn : Ti was attempted owing to the known volatility of K in the electron beam, which introduces undeterminable errors.

ID(1):  
ID(2):



### Section ESI-3 Solid-state $^{71}\text{Ga}$ NMR of **3**

$^{71}\text{Ga}$  magic angle spinning NMR spectrum acquired on a Bruker AVANCE I 300MHz spectrometer (95.6MHz  $^{71}\text{Ga}$  frequency) using a 2.5mm double resonance probe. A rotor synchronized Hahn echo sequence was used at a spinning frequency of 30kHz, radio frequency pulse amplitude equal to 100kHz and a relaxation delay of 1s. Chemical shift calibration was done with respect to 1M solution of  $\text{Ga}(\text{NO}_3)_3$  (aq) set at 0ppm.

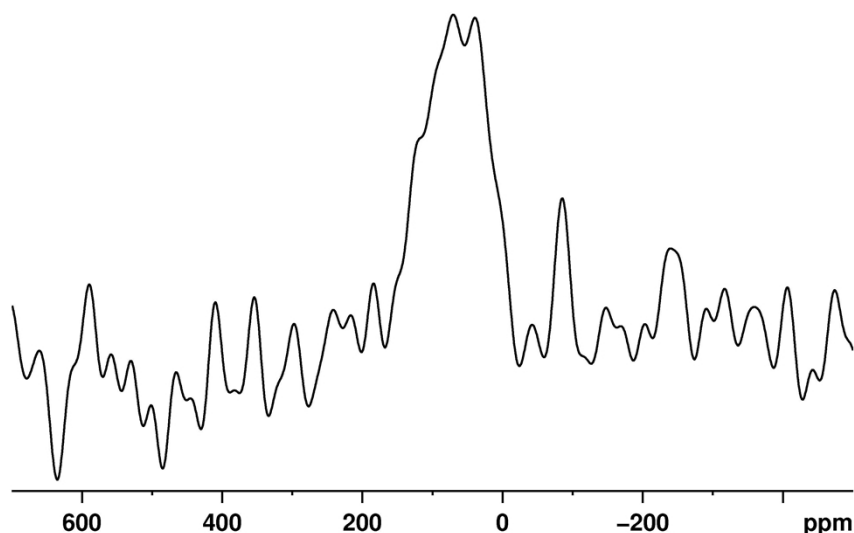


**Figure ESI-3.1** Solid state-MAS  $^{27}\text{Ga}$  NMR spectrum.

### Section ESI-4 Bond Valence Calculations

The formal oxidation state of the central Fe was investigated using Bond-Valence Sum calculations.<sup>1</sup> The valence of an individual bond between atoms  $i$  and  $j$  is given by  $S_{ij} = \exp((R_0 - R_{ij})/B)$  where  $R_0$  and  $B$  are unique parameters for a given metal and oxidation state and  $R_{ij}$  is the length of the bond. For this study  $B=0.37 \text{ \AA}$  in all cases. The valence (equivalent to the formal oxidation state) of the central atom is the sum of its individual bond valencies. Values for  $R_0$  suitable for  $\text{Fe}^{2+}$  in I.D. Brown's data compilation<sup>2</sup> are 1.734, 1.713 and 1.70  $\text{\AA}$  giving Fe valencies of 2.05, 1.94 and 1.87 respectively. Values for  $\text{Fe}^{3+}$  give valence sums of 1.759, 1.751 and 1.765  $\text{\AA}$  give valencies of 2.20, 2.15 and 2.23, respectively. Hence the formal oxidation state of the iron in this compound is clearly 2+. We checked the suitability of this approach by repeating the calculation for the gallium compounds, where the oxidation state must be 3+. Using  $R_0=1.730 \text{ \AA}$  for Ga-O and  $R_0=2.07 \text{ \AA}$  for Ga-Cl gives a valence of 2.63 for  $\text{Ti}_{14}\text{Ga}$ , which is rather low, and 2.89 for  $\text{Ti}_{14}(\text{GaCl})_2$ . We speculate that the low valence value for the interstitial Ga is a result of the tetrahedral hole being slightly larger than ideal for the small  $\text{Ga}^{3+}$  ion whereas there is no size constraint when the gallium is on the exterior of the cluster. We also note that the exo-cluster Ga-Cl bond has a higher valence (0.755) than any of the Ga-O bonds which are responsible for holding the Ga to the Ti-O framework (0.727, 0.709, 0.709).

For completeness we extended the analysis to  $\text{Ti}_{14}\text{Mn}$  cage **1**, confirming that this is a  $\text{Mn}^{2+}$  species with valency 1.94.

1. *The Chemical Bond in Inorganic Chemistry, The Bond Valence Model*. I.D. Brown, Oxford, **2002**

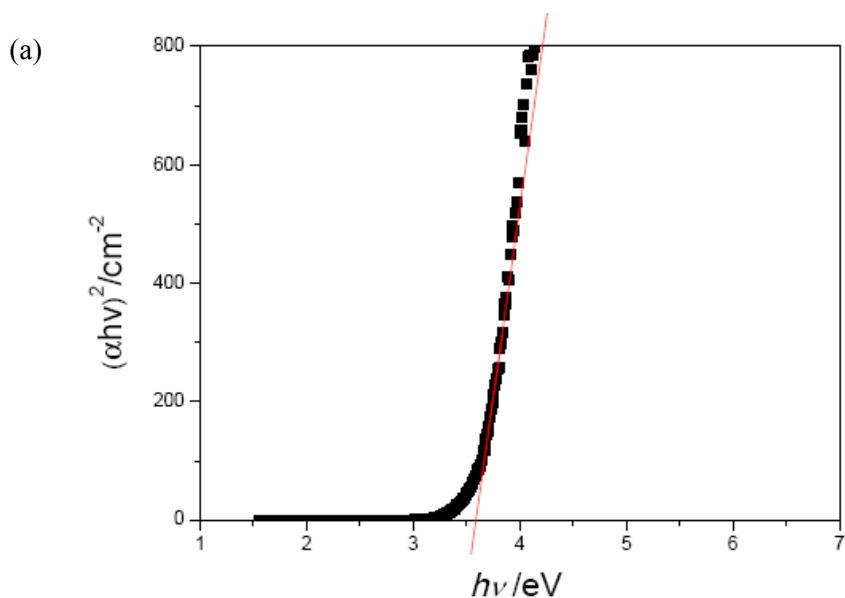
2. <http://www.iucr.org/resources/data/datasets/bond-valence-parameters>.

**Section ESI-5** Band Gap Calculations on **1**, **2**, **3**,  $[\text{Ti}_{16}\text{O}_{16}(\text{OEt})_{32}]$  and P25  $\text{TiO}_2$  Using a Direct Band Gap Semiconductor Model.

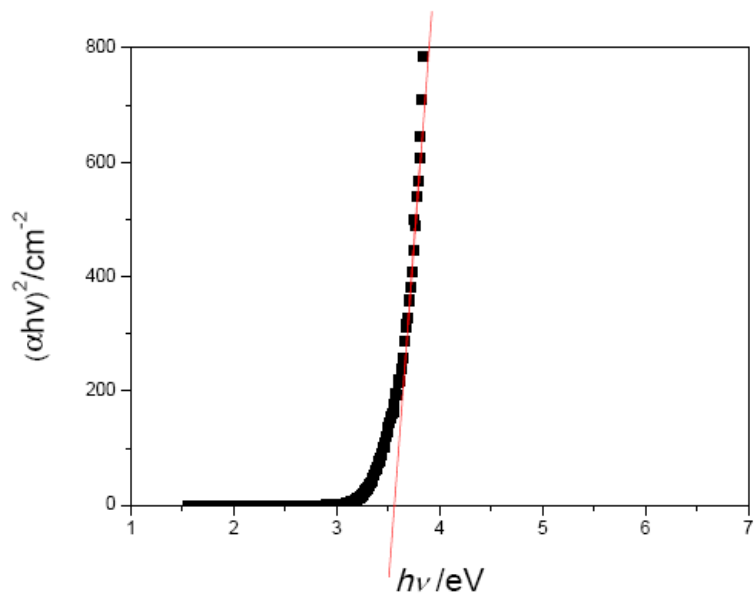
For a powdered direct band gap semiconductor material the equation below can be used to determine the band gap by plotting  $(\alpha h\nu)^2$  versus  $h\nu$  (see reference 18 of the paper).

$$(\alpha h\nu)^2 = C(h\nu - E_g)$$

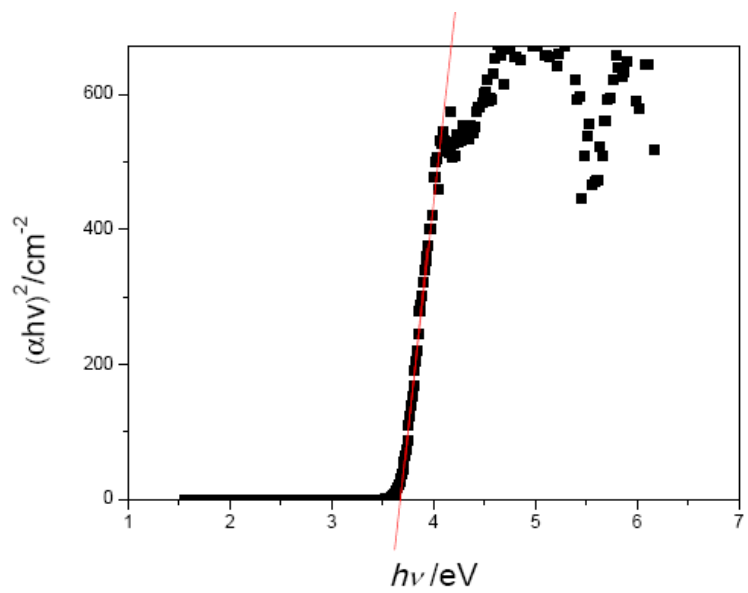
Where  $\alpha$  = the linear absorption coefficient [ $F(R)$ , the Kubelka-Munk function, for an infinitely thick material],  $C$  = a proportionality constant,  $h\nu$  = the photon energy and  $E_g$  = the band gap.

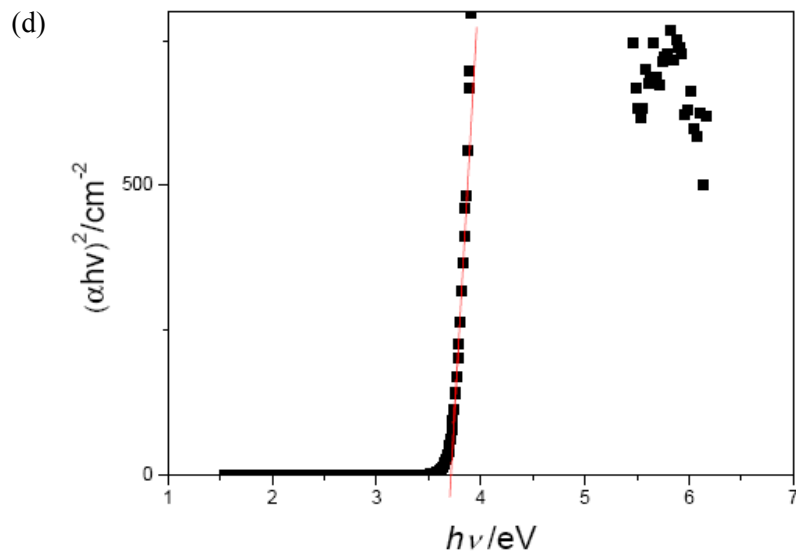


(b)



(c)

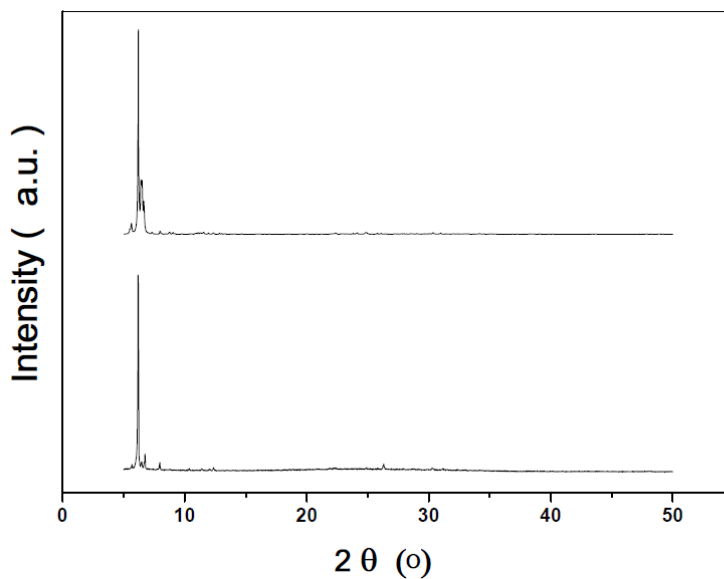




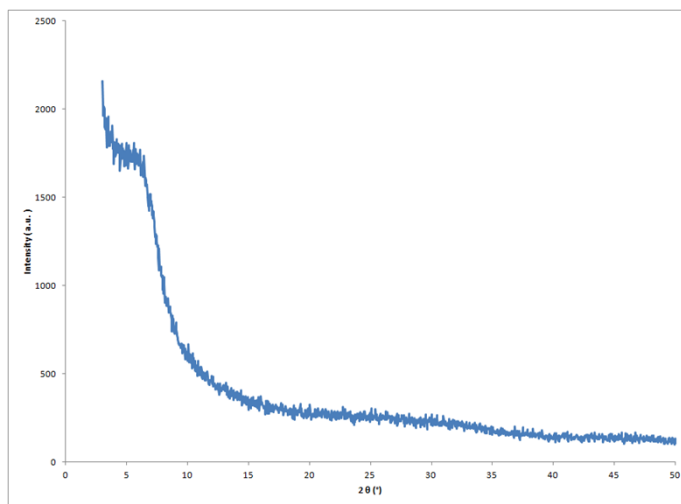
**Figure ESI-5.1** Band Gap Calculations on (a) **1** ( $E_g = 3.58$  eV), (b) **2** ( $E_g = 3.56$  eV), (c) **3** ( $E_g = 3.69$  eV), (d)  $[\text{Ti}_{16}\text{O}_{16}(\text{OEt})_{32}]$  ( $E_g = 3.73$  eV).

The band gap of P25  $\text{TiO}_2$  was determined by us previously using this model as 3.19 eV [(see Y. Lv, M. Yao, J. P. Holgado, T. Roth, A. Steiner, L. Gan, R. M. Lambert, *RSC Advances* 2013, **3**, 13659 (reference 7f of the paper)]. It was not re-determined in the current study.

**Section ESI-6** Powder XRD of Crystalline **5** and the Impurity Phase Present in the Reaction, Band Gap Determination of **5** (Using a Direct Band Gap Semiconductor Model) and Po

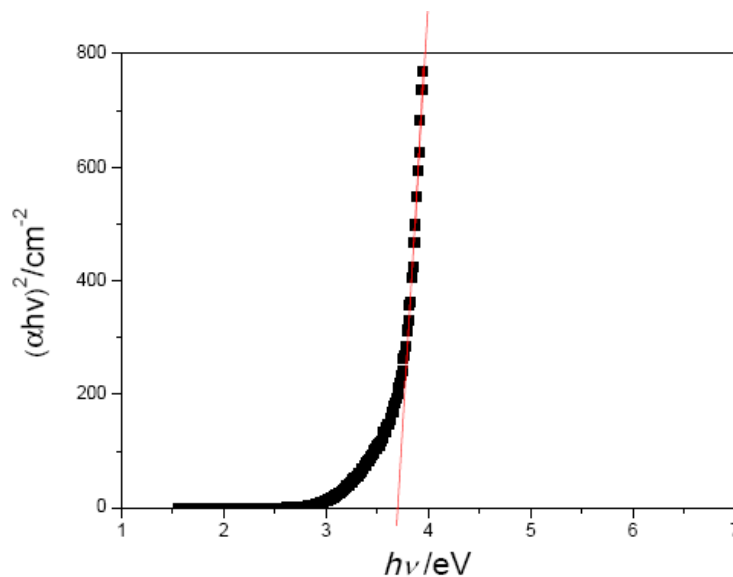


**Figure SI-6.1** The calculated powder XRD pattern for **5** (top) and the experiment pattern of **5** (bottom). Note that the absence of a rutile or anatase powder pattern is probably due to the low level of titania in **5** and to the amorphous nature of the impurity phase (see Figure SI-6.2, below).



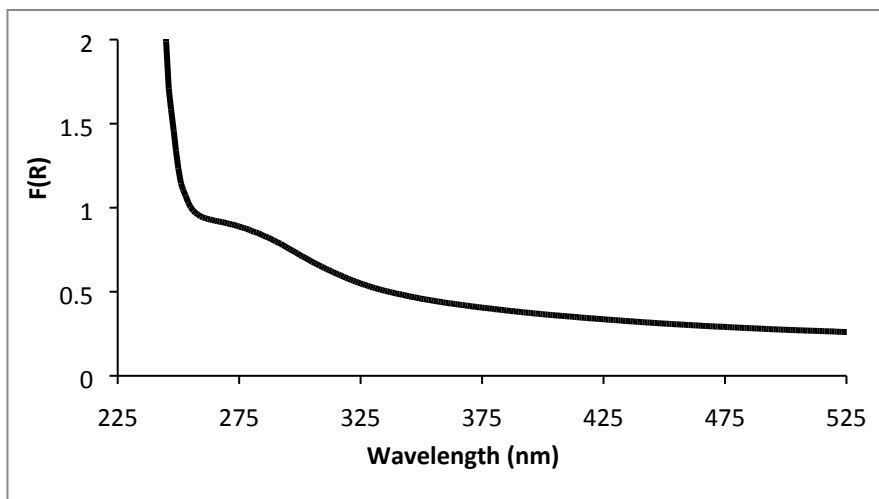
**Figure SI-6.2** Powder XRD pattern of the impurity present in the reaction producing **5**, showing that it is amorphous.

For comparison with Figure 7 of the paper, the band gap of **5** was determined using the direct band gap semiconductor model for completeness.



**Figure ESI-6.3** Band gap calculation for **5** ( $E_g = 3.79$  eV).

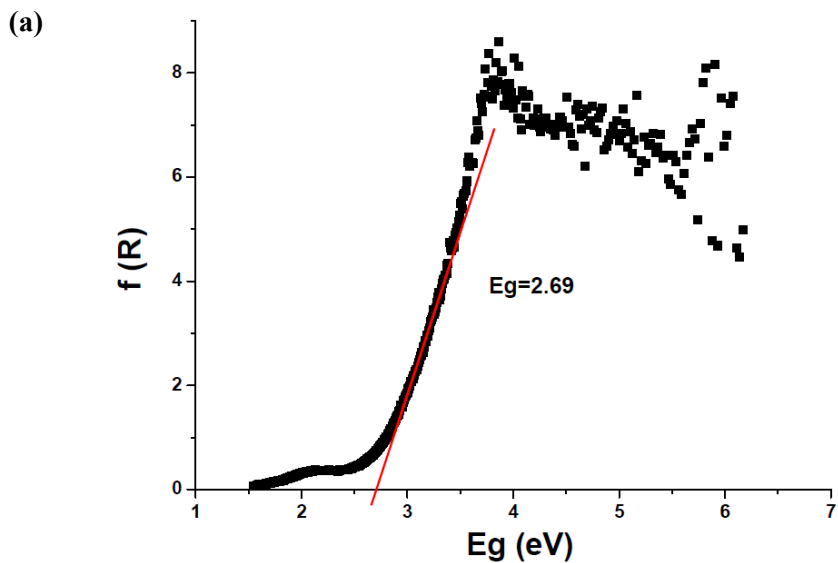
The values of 3.79 eV compares to 3.54 eV using the direct analysis of the absorption edge (see Figure 7 of the paper).



**Figure ESI-6.4** UV-visible spectrum of a saturated solution of **5** in EtOH.

### Section ESI-7 Band Gap and Powder XRD Measurements of Mn- and Fe-doped TiO<sub>2</sub>

Samples were prepared by hydrolysis of samples of **1**, **2** and **5** using a 50 : 50 EtOH solution, followed by sonication of the reaction solution, filtration of the solide produced and their calcination at 160 °C in air for 16 h. Powder XRD confirmed that these samples are contain the anatase phase and EDS analysis conformed that the samples contain Mn and Fe.



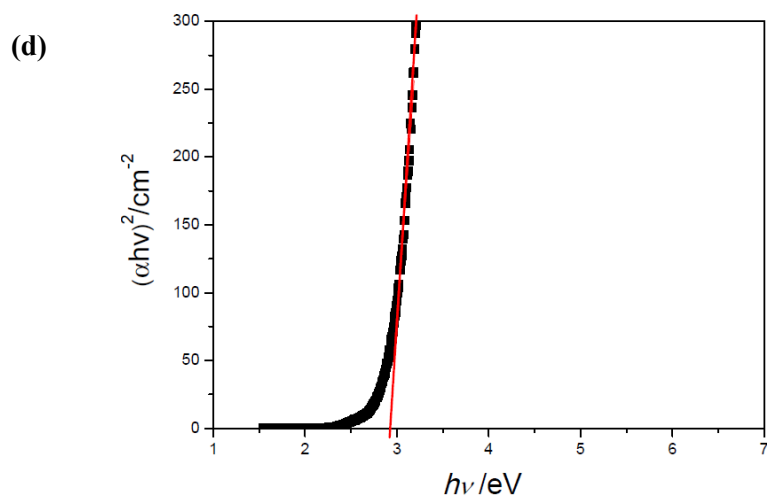
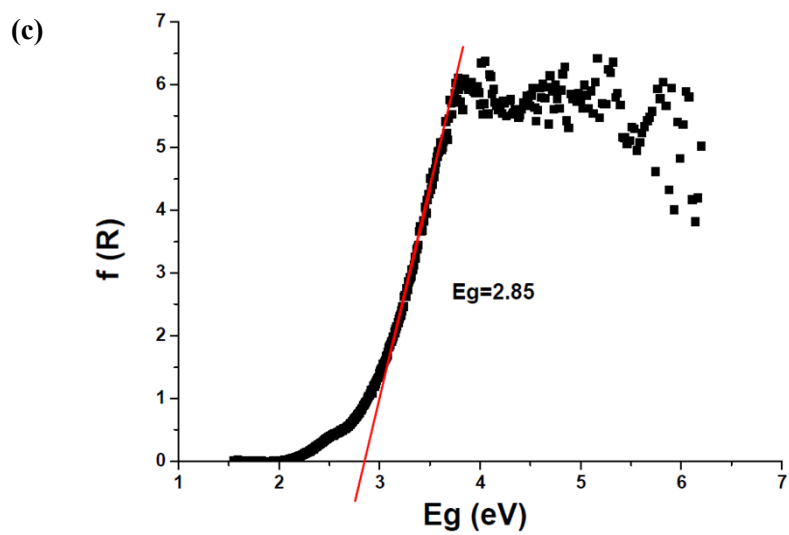
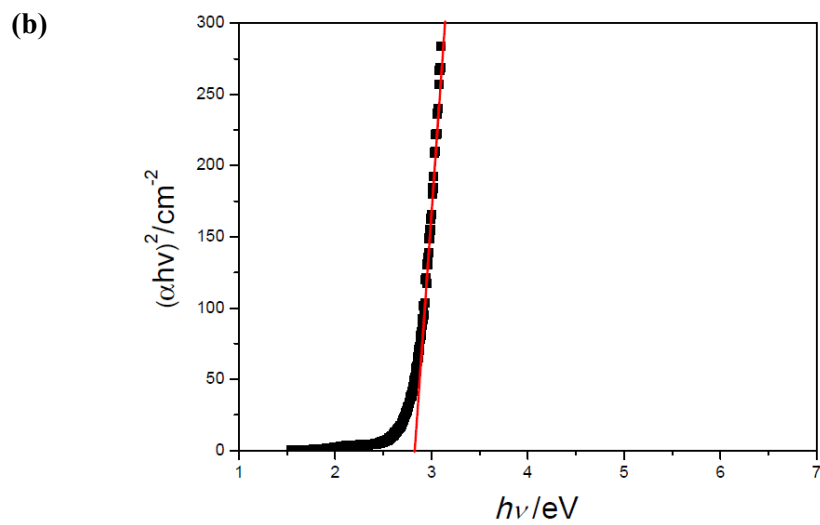


**Figure ESI-7.1** (a) Mn-doped TiO<sub>2</sub> using analysis of the absorption edge ( $E_g = 2.69$  eV), (b) Mn-doped TiO<sub>2</sub> using a direct band gap semiconductor model ( $E_g = 2.84$  eV), (c) Fe-doped TiO<sub>2</sub> ( $E_g = 2.85$  eV), (d) Fe-doped TiO<sub>2</sub> using a direct band gap semiconductor model ( $E_g = 2.99$  eV). Again the values differ by *ca.* 0.1-0.2 eV using the two methods of determining the band gap.

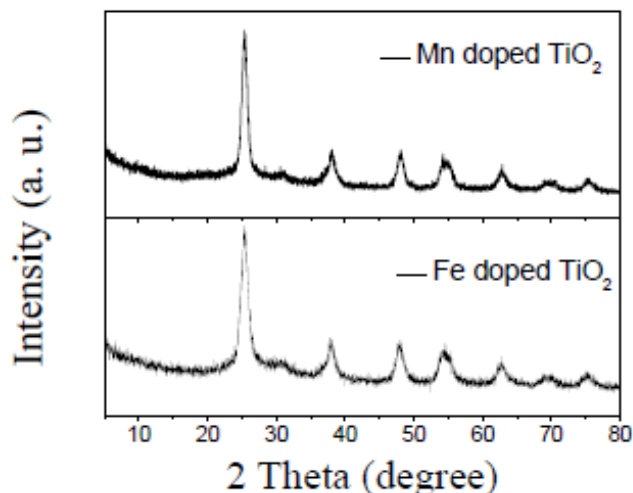
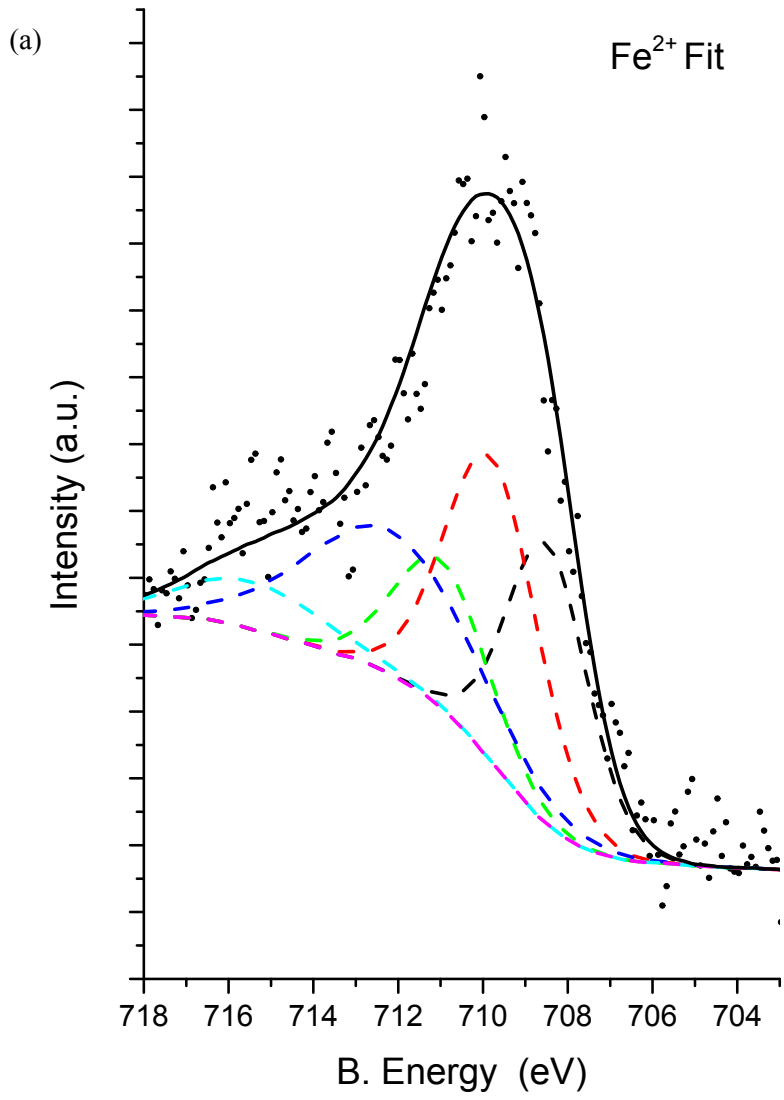


**Figure ESI-7.2** Powder XRD of Mn- and Fe-doped TiO<sub>2</sub>.

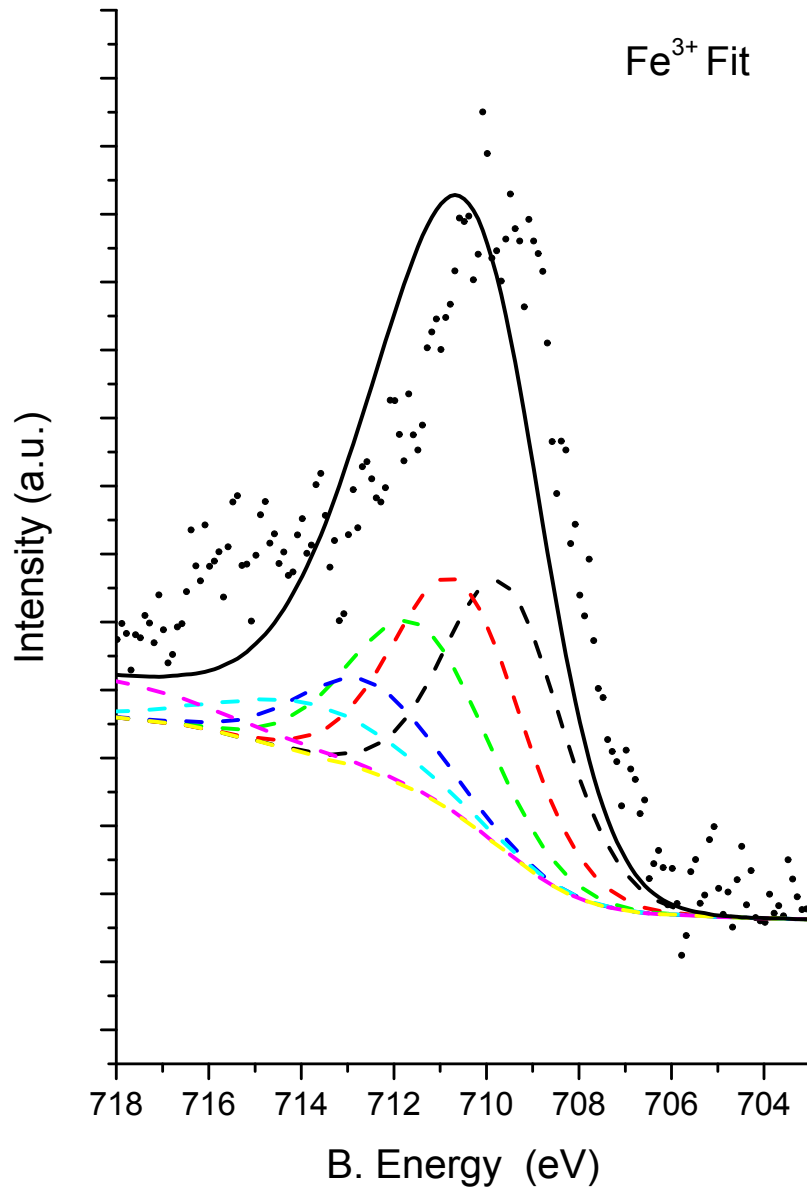
### Section ESI-8 XPS analysis of Samples 1, 2 and 5

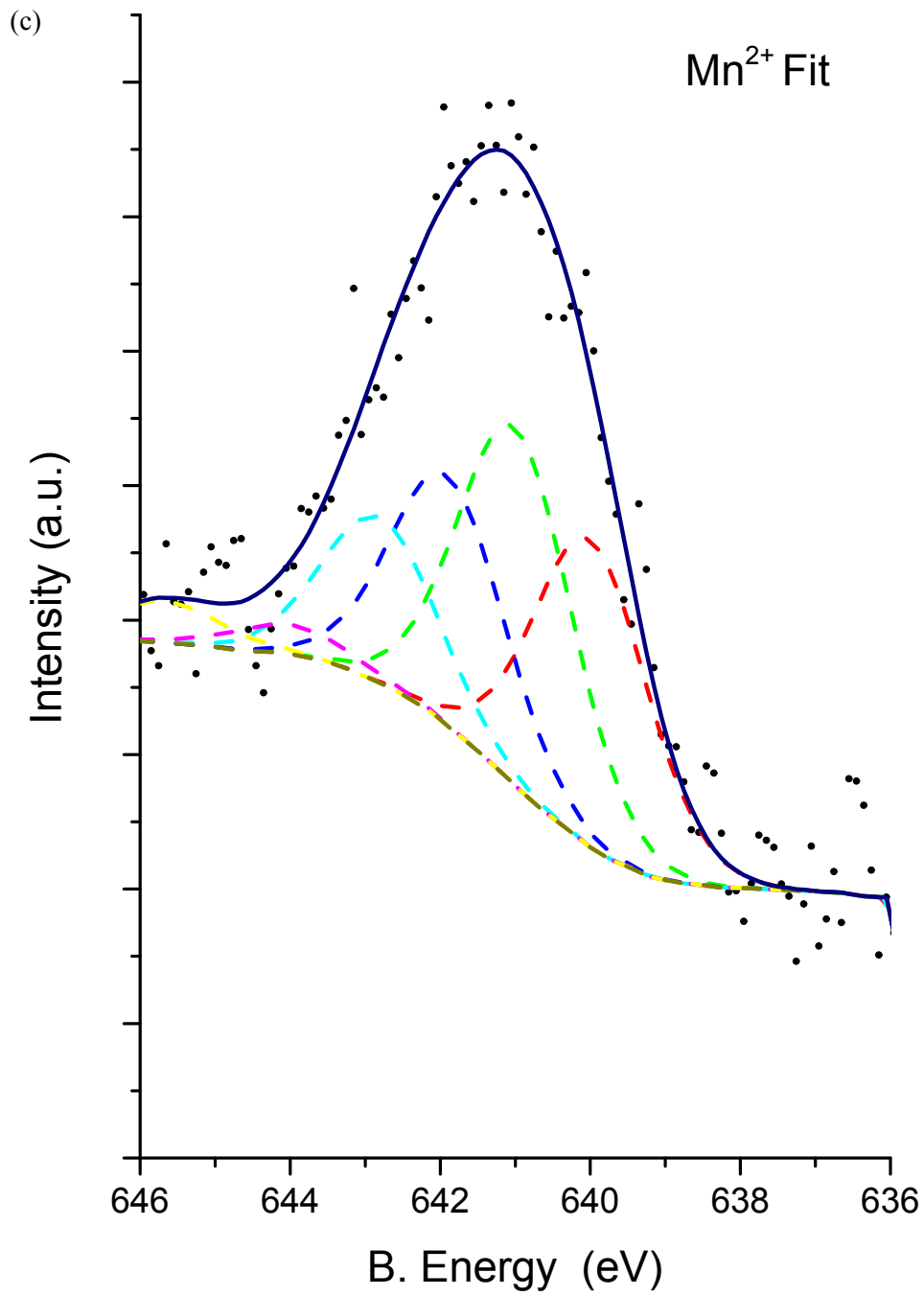
XP spectra were acquired at room temperature from a sample area of  $\sim 3 \times 3$  mm after evacuation to  $< 2 \times 10^{-9}$  mbar using a non-monochromated X-ray source and 50 eV analyzer pass energy. Spectra were analyzed by means of CasaXPS software with calibration based on reference Cu and Au principal peak positions using a standard Shirley background. Spectral fitting was non-trivial due to the multiplicity of possible oxidation states, some of which exhibit multiplet splitting. Binding energies, FWHM values, multiplet splitting values and peak weightings taken from the recent comprehensive compilation provided by Biesinger et al. were used to provide best fits for Fe<sup>2+</sup> versus Fe<sup>3+</sup> and Mn<sup>2+</sup> versus Mn<sup>3+</sup> (M.C. Biesinger, B.P. Payne, A.P. Grosvenor, L.W.M. Lau, A.R. Gerson, R.St.C. Smart, *Appl. Surf. Sci.* 2011, **257**, 2717).

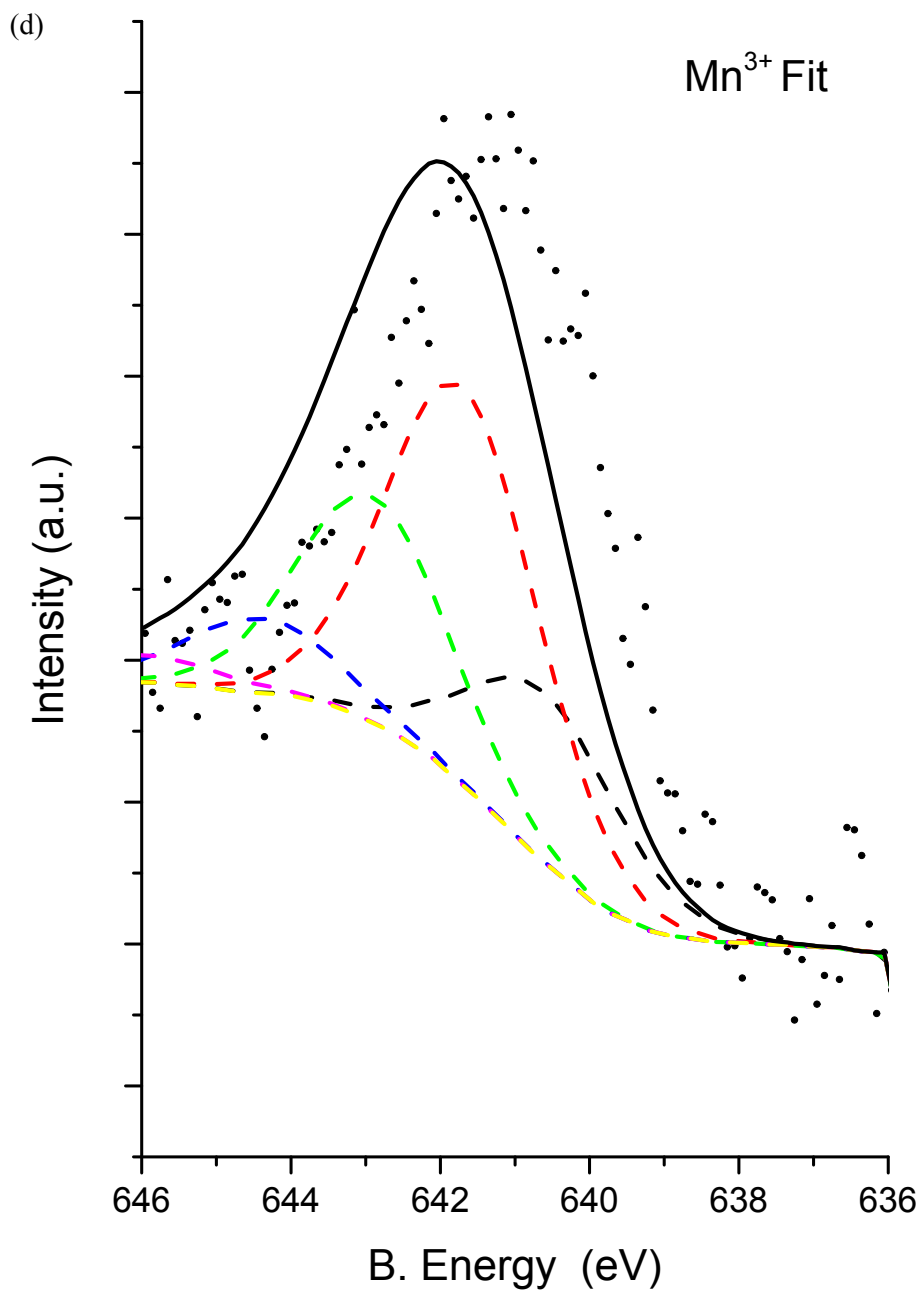
The results indicated that the oxidation states were Mn(II) in **1**, Fe(II) in **2** and Mn(II) in **5**.

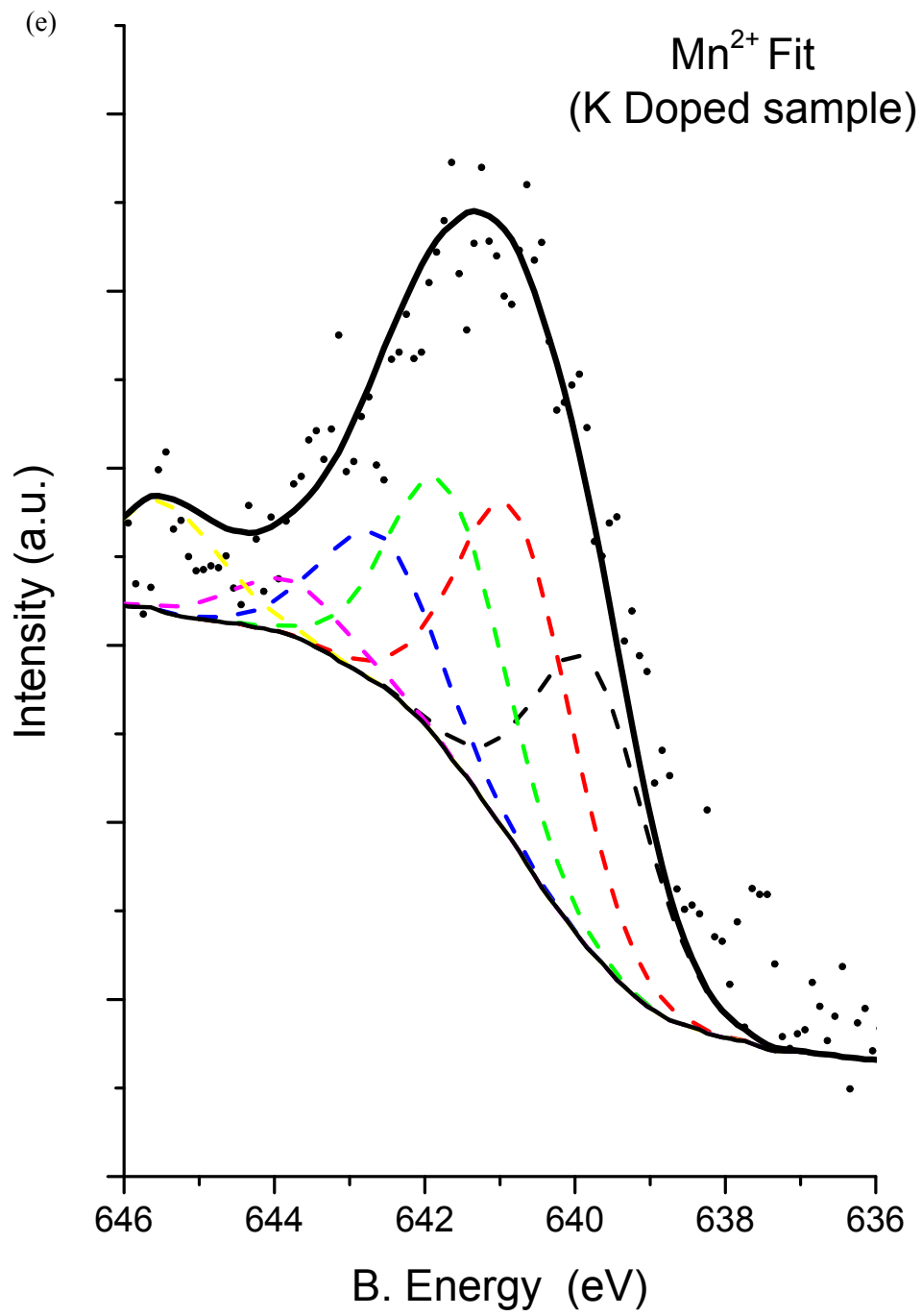


(b)









(f)

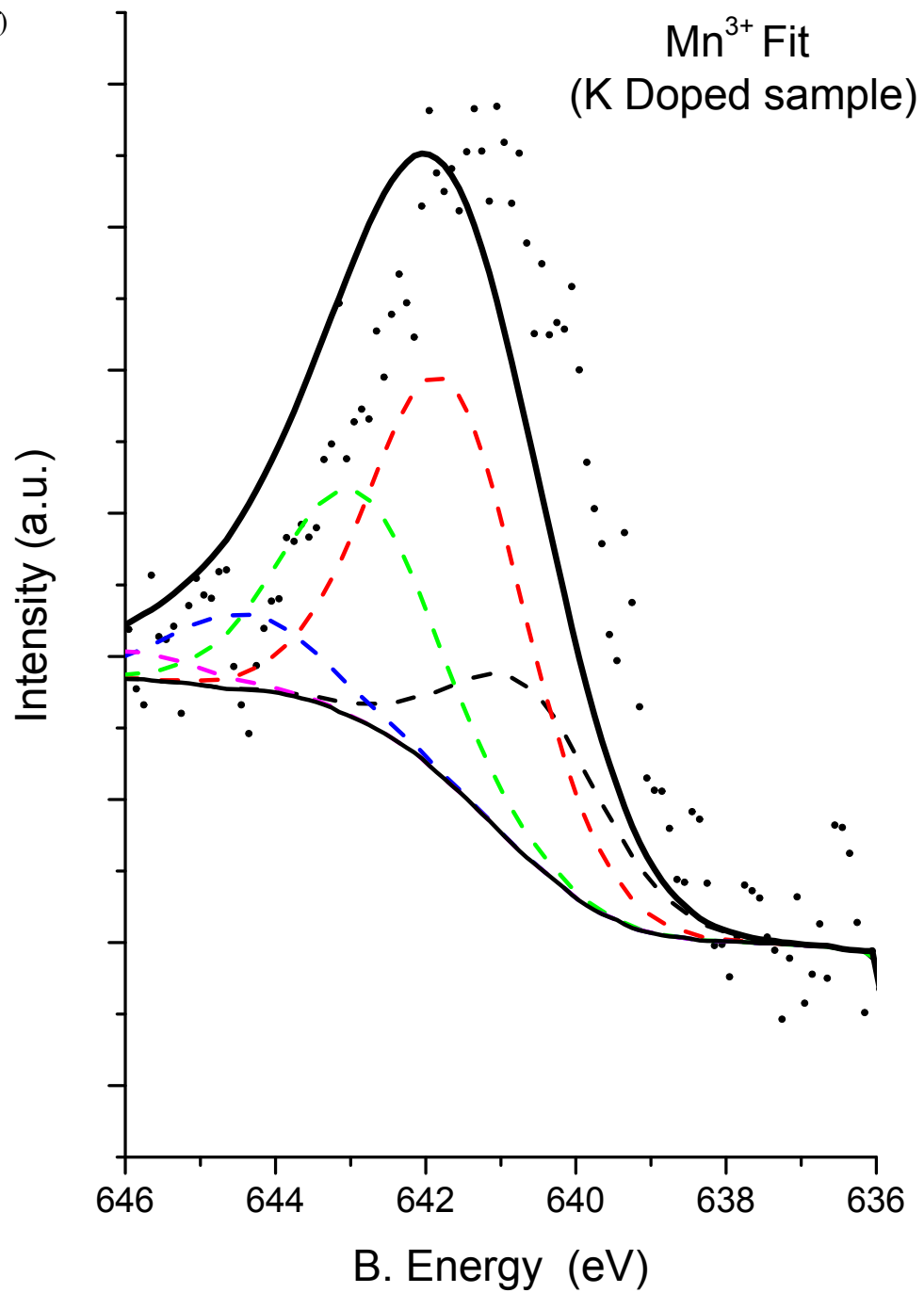


**Table 8.1** XPS Data: (a) and (b) – best-fit data for Fe<sup>II</sup> and Fe<sup>III</sup> for compound **2**; (c) and (d) – best-fit data for Mn<sup>II</sup> and Mn<sup>III</sup> for compound **1**; (e) and (f) – best-fit for Mn<sup>II</sup> and Mn<sup>III</sup> for compound **5**.

**Section ESI-9** DOS band gap calculations on the Mn<sup>III</sup>-doped cage [Ti<sub>28</sub>MnKO<sub>38</sub>(OEt)<sub>40</sub>].

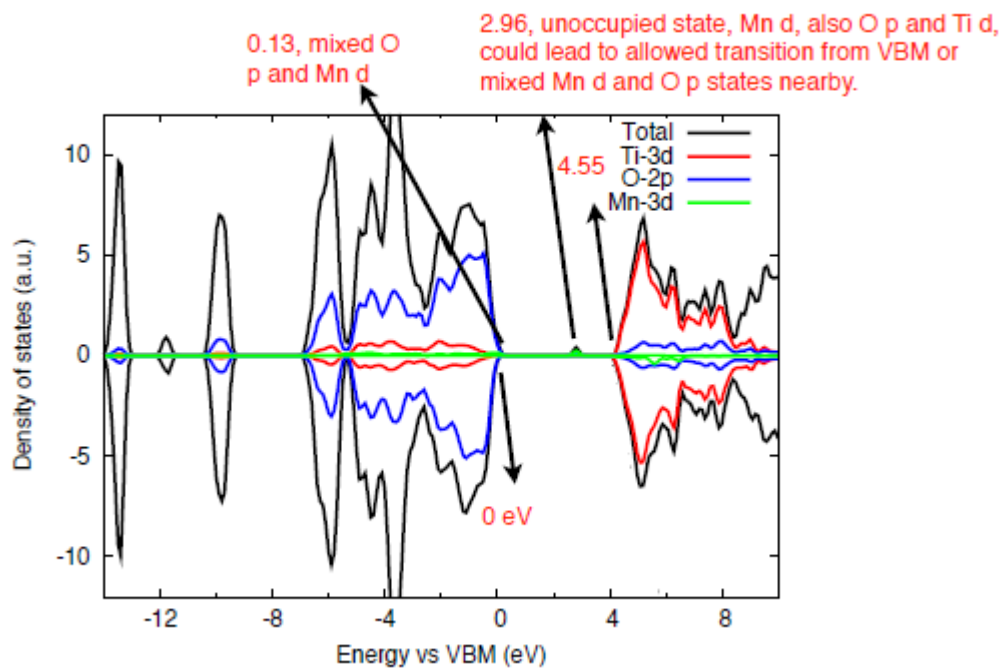


**Figure ESI 9.1** DOS calculation of the cage [Ti<sub>28</sub>MnKO<sub>38</sub>(OEt)<sub>40</sub>].